Environmental Science
Water Research & Technology

ROYAL SOCIETY OF CHEMISTRY

PAPER

View Article Online
View Journal | View Issue

Cite this: *Environ. Sci.: Water Res. Technol.*, 2024, **10**, 2997

Lead ion (Pb^{2+}) electrochemical sensors based on novel Schiff base ligands

Zahra Akbari,[a] Khouloud Abid,[ab] Daniela Iannazzo,[a] Morteza Montazerozohori,[c] Enza Fazio,[d] Fortunato Neri,[d] Carmelo Corsaro [d] and Giovanni Neri *[a]

In this study, a novel bidentate Schiff base ligand, namely (1*E*,1′*E*,2*E*,2′*E*)-*N*,*N*′-(butane-1,4-diyl)bis(3-(2-methoxyphenyl)prop-2-en-1-imine) (L^1), and a tetradentate Schiff base ligand, namely *N*1,*N*2-bis(2-(((1*E*,2*E*)-3-(4-(dimethylamino)phenyl)allylidene)amino)ethyl)ethane-1,2-diamine (L^2), were successfully synthesized through a simple procedure. The synthesized Schiff base ligands were characterized by scanning electron microscopy (SEM) analysis, attenuated total reflectance-Fourier transform infrared spectroscopy (ATR-FTIR), nuclear magnetic resonance (NMR) and ultraviolet-visible (UV-vis) spectroscopy. Moreover, the thermal behavior was studied through thermogravimetric (TG)/differential thermogravimetric (DTG)/differential thermal (DT) analyses under a nitrogen atmosphere. Subsequently, the features and performances of the synthesized ligands (L^1 and L^2) as electrochemical sensors for the detection of heavy metal ions (HMIs) have been investigated. A different behavior was noticed using these two ligands, with L^1 being the best candidate for developing a modified screen-printed carbon electrode (L^1/SPCE) electrochemical Pb^{2+} sensor. To improve further the performances, gold nanoparticles (AuNPs) were deposited by an electrochemical process on the L^1/SPCE platform. The developed AuNPs-L^1/SPCE sensor displayed enhanced lead ion sensing with a high sensitivity of 56.78 μA μM^{-1} cm^{-2} and a detection limit of 0.298 μM. This novel sensor demonstrated promising performances for the detection of Pb^{2+} ions in real seawater with no sample treatment.

Received 9th June 2024,
Accepted 11th September 2024

DOI: 10.1039/d4ew00485j

rsc.li/es-water

Water impact

A new electrochemical sensor was developed by combining AuNPs with a Schiff base ligand. This generated a synergistic effect that was exploited for improving the electrochemical sensing performances for the detection of Pb^{2+} in the sub-micromolar range. The feasibility of the proposed platform for practical applications in the environmental field was confirmed by determining Pb(II) in seawater.

Introduction

Schiff bases are unique ligands that play an essential role in the development of coordination chemistry. They are easily synthesized and can be readily modified both electronically and sterically.[1] Schiff bases form an outstanding class of ligands due to their unique properties such as stability under different conditions, diversity of donor sites, synthetic flexibility, and formation of a wide range of complexes in various coordination geometries. Schiff base ligands based on the number of donor sites are classified as monodentate, bidentate, tridentate, and so on. Various bidentate and tetradentate Schiff base ligands have been prepared from condensation reactions of different aldehydes and amines.[2–6] Also, Schiff bases having tetradentate ligands are known to exhibit good fluorescence properties and high thermodynamic and kinetic stability.[7–10] Schiff bases emerge as attracting ligands for binding with heavy metal ions (HMIs). Various studies have shown good affinity of the nitrogen atom in the azomethine group for metal ions. The mechanism of electrochemical sensors for monitoring metal ions is based on the adsorption of metal ions from solution to the electrode surface by complexation with the ligand immobilized on the working electrode.[11] Hence, the choices

[a] *Department of Engineering, University of Messina, I-98166 Messina, Italy. E-mail: sanazakbari701@yahoo.com, khouloud.abid.etud@fss.usf.tn, diannazzo@unime.it, gneri@unime.it*
[b] *CNR IPCF Istituto per i Processi Chimico-Fisici, viale F. Stagno D'Alcontres 37, Messina, Italy*
[c] *Department of Chemistry, Yasouj University, Yasouj, Iran. E-mail: mmzohory@yahoo.com*
[d] *Department of Mathematical and Computational Sciences, Physics Science and Earth Science, University of Messina, Viale F. Stagno d'Alcontres 31, I-98166 Messina, Italy*

of materials to modify the working electrode are of great importance, and Schiff bases are reported to be an excellent choice for fabricating metal ion sensors due to their good selectivity. Furthermore, their capability for the accumulation of metal ions at the electrode surface results in the voltammetric determination of low detection limits.[12–16]

Environmental pollution by heavy metal ions is a serious and complex problem.[17–20] Among various HMIs, lead ions (Pb^{2+}) are one of the most serious environmental contaminants because of their high toxicity, persistence, and tendency to accumulate in living organisms.[21,22] The detection and monitoring of Pb^{2+} in water environments, especially seawater, are crucial for environmental protection and public health.[23] Therefore, it is desirable to develop simple, selective, sensitive, and efficient methods for the determination of Pb^{2+} ion trace levels in environmental samples. In the past few years, plenty of detection methods have been established for the detection of Pb^{2+}, including spectrophotometric methods, atomic absorption and emission spectroscopies, and mass spectrometry (MS).[24–27] However, most of these techniques are either time-consuming, involving multiple sample manipulations, or highly expensive for most analytical laboratories.

To bypass these limitations, electrochemical sensors have been widely used in the determination of various substances due to their ease of use, low cost, high sensitivity, and desirable selectivity in their responses.[28–31] Ahmed *et al.*[32] proposed an electrochemical sensor by functionalizing the working electrode with a freshly synthesized Schiff base, 4-((2-hydroxy-5-((4-nitrophenyl)diazenyl)benzylidene)amino)benzoic acid (HDBA) and used it for simultaneous determination of lead (Pb^{2+}), copper (Cu^{2+}) and cadmium (Cd^{2+}) ions in a buffer solution of 0.1 M Tris-HCl. Interestingly, the authors reported that the addition of Pb^{2+} to a solution containing Cd^{2+} has an insignificant effect on the Cd^{2+} peak current which implies that this Schiff base endows extra selectivity to the modified electrode and avoids mutual interference during simultaneous determination of the heavy metals. In the study of Kumar Saren *et al.*,[33] the Katiragum–Arginine Schiff base material is used as a sensor–adsorbent for Pb^{2+} in an aqueous solution. The sensing of Pb^{2+} is analyzed by the electrochemical method with a detection limit of 0.146 μM. The Schiff base/glassy carbon electrode (KGDR/GCE) is highly selective towards Pb^{2+} ions in comparison to other environmentally relevant ions as well as in water samples. Chandra *et al.*[34] developed a new Pb^{2+} PVC membrane sensor based on Schiff base thiophene-2-aldehyde thiosemicarbazone (TATS) as an ionophore, tetraphenylborate (NaTPB) in the form of an anion excluder and dioctyl phthalate (DOP) as a plasticizer. The sensor exhibits good selectivity to a wide variety of alkali, alkaline earth, and other metal ions and works over a pH range of 2.4–8.0. A highly selective graphene/Schiff base fluorescent chemosensor for iron ions was developed by modification of functionalized graphene oxide with a naphthaldehyde–diaminobenzophenone Schiff base.[35] The detection limit of this sensor for Fe^{2+} and Fe^{3+} was found to be 0.277×10^{-5} mol L^{-1} and 0.337×10^{-5} mol L^{-1}, respectively. The lower detection limit of this sensor for Fe^{2+} and Fe^{3+} ions proved its application in the sensing phenomenon and showed its sensitivity.

In this work, two Schiff bases named L^1 and L^2 were successfully synthesized through a simple procedure. Using several techniques, their morphological, optical and electrochemical features were studied. These two ligands have been then used to prepare two electrodes for the determination of Pb^{2+} ions in PBS at pH = 9 using the square wave voltammetry (SWV) technique. The sensitivity increased through the electrochemical deposition of AuNPs on the surface of the modified electrode and the obtained detection limit is equal to 0.298 μM.

Results and discussion

L^1 and L^2 ligand characterization

The Schiff base ligands (L^1) and (L^2) synthesized according to a previously reported procedure[36] have been characterized by several techniques for elucidating and confirming their chemical structure. FTIR spectra within the wavenumber range of 4000–400 cm^{-1} are reported in Fig. 1. As noticed, the spectrum of Schiff base ligand L^1 (black line) shows the characteristic stretching frequency of the azomethine group at 1631 cm^{-1}.[2] Moreover, the absorption bands appearing at 3000 cm^{-1}, 2931 cm^{-1}, and 1164 cm^{-1} are attributed to the vibrations of ν(C–H) alkene, ν(C–H) aliphatic, and ν(C–N) bonds in the ligand (L^1), respectively.

Regarding the L^2 Schiff base ligand (red line), at 1600 cm^{-1} and 1629 cm^{-1}, the symmetric and asymmetric stretching frequencies of the azomethine (C═N) group are observed, respectively. Additionally, the absorption bands appearing at 3088 cm^{-1}, 2923 cm^{-1}, and 1159 cm^{-1} are assigned to the stretching vibrations of ν(C–H) alkene, ν(C–H) aliphatic, and ν(C–N) bonds, respectively. Furthermore, a stretching vibration is noticed at 3215 cm^{-1} which corresponds to the ν(N–H) bond.

The molecular structure of the prepared Schiff base ligands was demonstrated through ^{1}H NMR and ^{13}C NMR analyses in deuterated DMSO solution, and the obtained spectral data are depicted in Fig. 2.

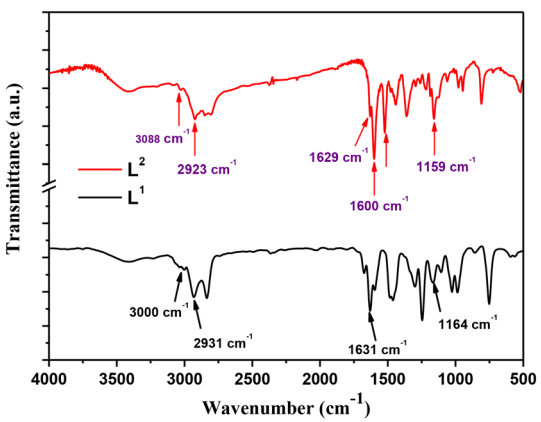

Fig. 1 FT-IR spectra of Schiff base ligands L^1 (black line) and L^2 (red line).

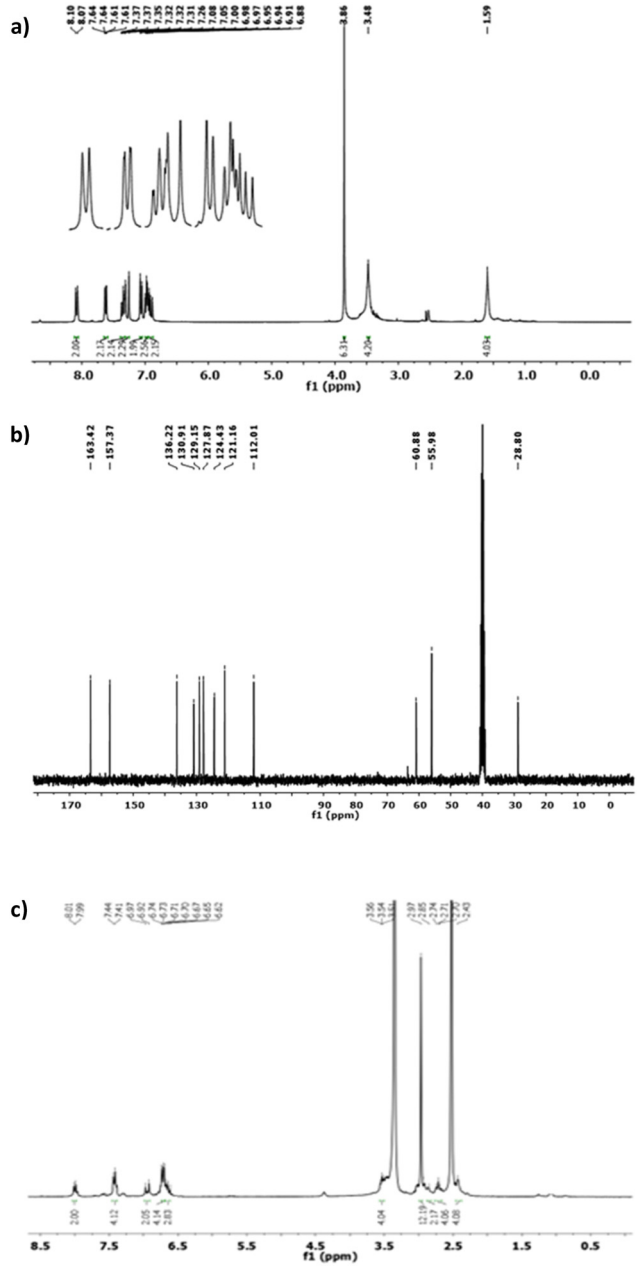

Fig. 2 The ^{1}H NMR (a) and ^{13}C NMR spectra (b) of the Schiff base ligand L^1. (c) ^{1}H NMR spectrum of L^2.

As shown in Fig. 2a, among the significant proton signals in the ^{1}H NMR spectrum, the azomethine proton signal in the L^1 ligand (HCC′) appears as a doublet at 8.08 ppm. The aromatic hydrogens (Hff′, Hgg′, Hhh′, and Hii′) exhibit signals as a doublet of the doublet, triplet, doublet of triplet, and doublet at 7.62, 6.98, 7.35, and 7.06 ppm, respectively.

In the ^{13}C NMR spectrum of ligand L^1, the carbon signals corresponding to aromatic, aliphatic, and olefinic carbons are observed within the ranges of 121.16–157.37 ppm, 28.8–55.96 ppm, and 112.01–136.22 ppm, respectively (see Fig. 2b). The distinctive carbon signal in the bidentate ligand (L^1) is attributed to the azomethine carbon peak, which appears at 163.42 ppm. Regarding the ^{1}H NMR spectrum of ligand L^2 reported in Fig. 2c, the olefinic hydrogens (Hdd′ and Hee′) are observed as a doublet of doublet and a doublet, centered at 6.92 ppm and 7.28 ppm, respectively. Two broad singlet signals at 1.59 ppm and 3.45 ppm are assigned to the aliphatic hydrogens of Haa′ and Hbb′, respectively.

Photoluminescence (PL) and ultraviolet-visible (UV-vis) absorbance spectra were used to investigate the optical properties of both L^1 and L^2 ligands, as shown in Fig. 3.

The UV-vis spectra of ligand L^1 (black line) and ligand L^2 (red line) are collected at room temperature in the range of 200–800 nm. In Fig. 3a, two distinct UV-vis intra-ligand transition bands were observed exhibiting maximum absorption (λ_{max}) values at 280 nm and 325 nm, respectively. The first one is attributed to the $\pi \rightarrow \pi^*$ electronic transition involving olefinic bonds and aromatic rings.[36] On the other hand, the 325 nm band was assigned to the $n \rightarrow \pi^*/\pi \rightarrow \pi^*$ transitions associated with iminic bonds.[36]

Fig. 3b shows the UV-vis optical absorbance spectra of ligand L^2, which exhibited two characteristic intra-ligand transitions centred at the λ_{max} of 322 nm and 399 nm. The band observed at 322 nm corresponds to $\pi \rightarrow \pi^*$ electronic transitions involving olefinic bonds and aromatic rings, whereas the band observed at 399 nm is attributed to $n \rightarrow \pi^*/\pi \rightarrow \pi^*$ transitions of iminic bonds.

Fig. 3c shows the PL spectra of both L^1 (black line) and L^2 (red line) ligands collected under 390 nm excitation at room temperature. Herein, the spectra of both Schiff base ligands are dominated by a characteristic emission peak of the L^1 ligand centred at about 450 nm in agreement with G. Wu,

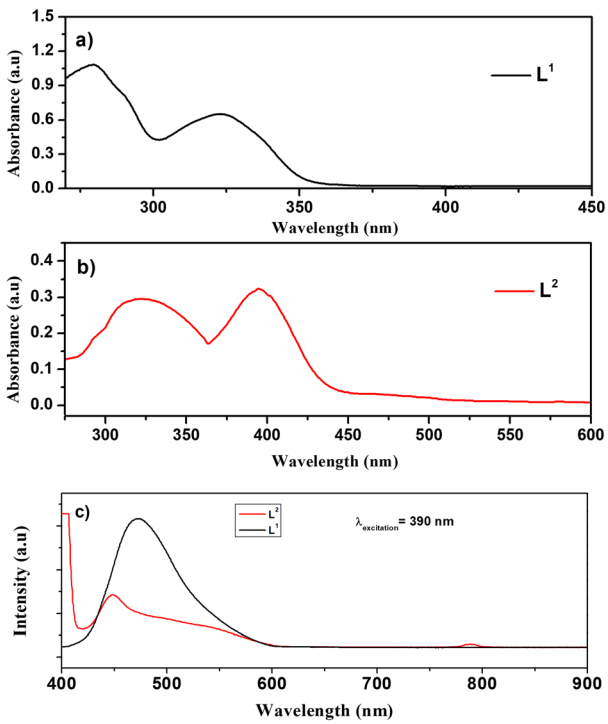

Fig. 3 UV-visible spectra of (a) L^1 and (b) L^2 ligands. (c) PL spectra of the Schiff base ligands; L^1 (black line) and L^2 (red line).

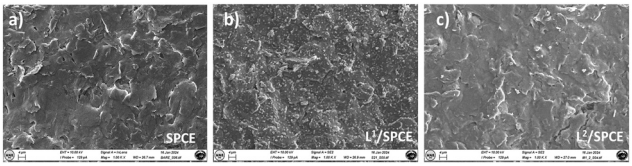

Fig. 4 SEM images of the working electrode on the bare (a), L^1 (b) and L^2 (c) SPCEs.

et al.[37] Moreover, a shoulder is observed at 550 nm for ligand L^2; also, the second harmonic at 780 nm can be observed.

Modified-SPCE characterization

The L^1 and L^2 ligands were then used to fabricate modified-SPCEs, as reported in the Experimental section. Fig. 4 displays the SEM analysis of the working electrode surface of the bare and L^1 and L^2 ligand-modified SPCEs. The images show clearly that the working electrode surface is almost covered by a continuous film of the L^1 and L^2 ligands. In the case of the L^1 film, a homogeneous distribution of small structures with a particle-like shape is also observed which is absent on the L^2 film.

The high resolution image in Fig. 5a shows the porous structure of the L^1 ligand modified-SPCE. Fig. 5b also shows the surface of the AuNPs-L^1/SPCE working electrode. The image highlights the presence of uniformly distributed AuNPs seen as white round nanoparticles having a mean size lower than 30 nm.

To investigate the electrochemical characteristics of the bare SPCE and other modified SPCEs (L^1/SPCE, L^2/SPCE, and AuNPs-L^1/SPCE), cyclic voltammetry (CV) and EIS tests were performed in 0.1 mol L^{-1} KCl solution containing 5 mM $Fe(CN)_6$. CV analysis in the presence of the model ferrocyanide/ferricyanide redox couple provides valuable information about the involved redox process. Comparative CV analysis reported in Fig. 6a indicated that the redox couple process feasibility follows the order AuNPs-L^1/SPCE > SPCE = L^1/SPCE > L^2/SPCE, which can be due to the improved microstructural and electrical characteristics (*e.g.*, surface area, metal particle presence, hydrophilicity, porosity, electron transfer resistance) introduced by modifying the bare electrode. EIS is a tool for investigating the electrode interface properties in terms of impedance changes, over a wide range of applied frequency. This technique can provide helpful indication on the electrical characteristics of the electrode–solution interface. The Nyquist plot of each electrode is presented in Fig. 6b, showing a semi-circle and a linear portion.[38–40] Using the Nova software, the obtained Nyquist plots were fitted through the equivalent circuits in Fig. 6c and d. The Randles parameters, *i.e.* the charge transfer resistance (R_{CT}) and electrolyte resistance (R_s), were calculated and are compared in Table 1.

The order of R_{CT} established: L^1/SPCE < AuNPs-L^1/SPCE < SPCE < L^2/SPCE displays a different trend compared to one based on CV data, suggesting that the electron transfer resistance is not the only parameter taken into account for the electrochemical characteristics of the electrodes.

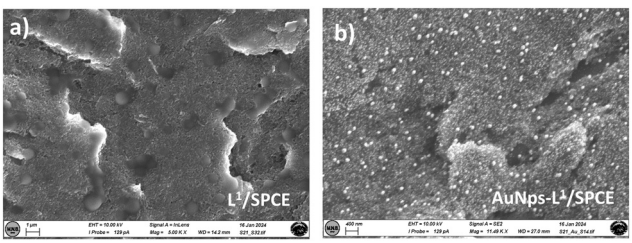

Fig. 5 High-resolution SEM images of the L^1 sample without (a) and with AuNPs (b).

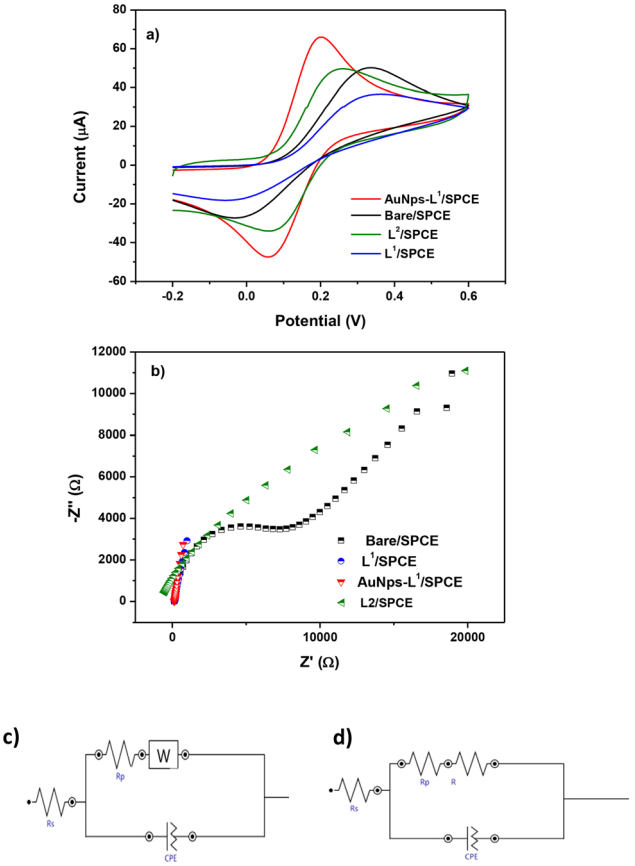

Fig. 6 (a) CV test, (b) Nyquist plots in $[Fe(CN)_6]^{3-/4-}$ solution for bare/SPCE (black line), L^1/SPCE (blue line), L^2/SPCE (green line), and AuNPs-L^1/SPCE (red line) electrodes. (c) The equivalent circuits of bare/SPCE, L^1/SPCE, and L^2/SPCE electrodes and (d) AuNPs-L^1/SPCE.

Table 1 Randles parameters obtained from fitting using Nova software

	Randles parameters	
Sensor	R_{CT} (Ω)	R_s (Ω)
Bare/SPCE	14 692	156
L^2/SPCE	47 199	179
L^1/SPCE	83	133
AuNPs-L^1/SPCE	490	1221

At last, as demonstrated by the combined data of CV in ferrocyanide and EIS analysis, the AuNPs-L1/SPCE sensor displays the best electrochemical properties as evidenced by the values of the two key parameters *i.e.* high I_{pa} and low R_{CT}, respectively.

Electroanalytical performance toward Pb^{2+}: parameter optimization

The determination of Pb^{2+} ions by SWASV was carried out with the investigated sensors. To obtain better sensitivity, the operating conditions of SWASV, *i.e.* pH, deposition potential (V_{dep}), and deposition time (t_{dep}), were first optimized (Fig. 7).

The effect of V_{dep}, from −0.2 V to −1.0 V, in acetate buffer solution (pH = 2.35) containing 3.6 μM of Pb^{2+} on the anodic current peak is reported in Fig. 7a. Decreasing the deposition potential up to −1.0 V clearly increases the Pb^{2+} peak current. H_2 bubble production was noted at a lower potential than −1.0 V, which could be a potential destabilizing factor for the film adhesion on the working electrode sensor. Therefore, the deposition potential value of −1.0 V was selected.

The pH of the acetate buffer solution should be also optimized to have a better electroanalytical response in the Pb^{2+} determination. To achieve this, three different media were chosen: acidic (pH = 4), neutral (pH = 7), and basic (pH = 9). The effect of pH on the determination of the Pb(II) ions is presented in Fig. 7b. At pH 4.0, the peak current reached the maximum for Pb^{2+} while a poorer result was obtained in the neutral medium. In the basic medium, the Pb^{2+} ions are monitored with an intensity 3 times higher than that obtained at pH = 7, but almost 5 times lower than that noticed at acidic pH. However, since the target of this work is the detection of heavy metals in seawater, the value of pH = 9 is selected.

For heavy metal ion determination at low concentrations, generally a long deposition time (t_{dep}) is selected which ensures the deposition of more lead ions on the working electrode surface. In this work, we select a deposition time of 600 s. To sum up, the parameters selected for the successive Pb^{2+} analysis tests were: t_{dep} = 600 s, V_{dep} = −1.0 V, and pH = 9.

Electroanalytical performance toward Pb^{2+} on L^1/L^2-based modified SPCEs

The results of SWASV tests for the determination of lead ions are reported in Fig. 8. The typical current variation registered during the SWASV test in the potential range between −0.9 and −0.4 V is illustrated in Fig. 8a. From the current variation *versus* the addition of an increasing quantity of lead ions in the calibration curves, it appears that the modified L^1/SPCE electrode provides the highest sensitivity to Pb^{2+} compared to bare SPCE and L^2/SPCE.

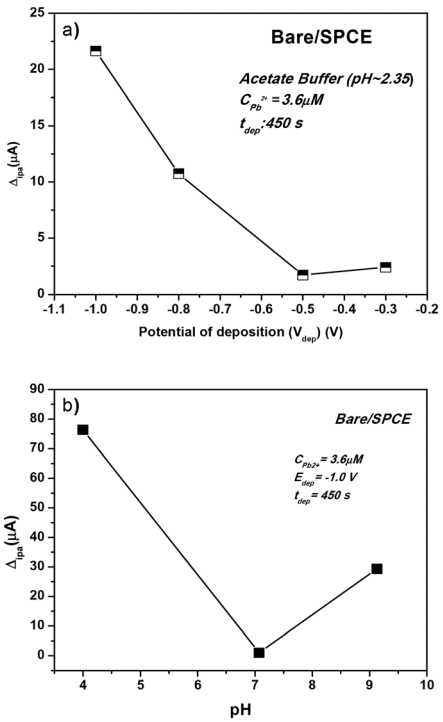

Fig. 7 (a) Potential deposition (V_{dep}) optimization on bare/SPCE toward the determination of Pb^{2+} in acetate buffer solution (pH = 2.35); (b) pH optimization of acetate buffer solution on bare/SPCE at 3.6 μM of Pb^{2+}.

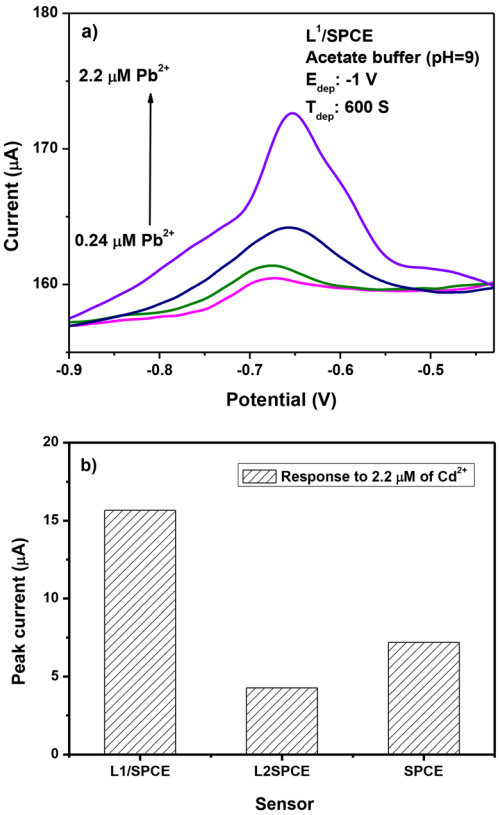

Fig. 8 (a) SWASV voltammograms of L^1/SPCE registered in an acetate buffer solution containing a low concentration of Pb(II) ions; conditions: pH = 9.0, E_{dep} = −1.0 V, and t_{dep} = 600 s. (b) Response of the bare and modified-SPCE sensor to Cd ions.

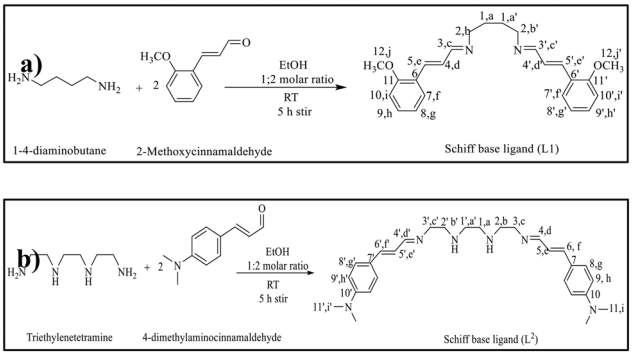

Scheme 1 Synthesis of Schiff base ligands (a) L^1 and (b) L^2.

The best performance of L^1/SPCE, compared to bare SPCE, may be attributed to the presence of bidentate C═N groups in the chemical structure of the L1 ligand (see Scheme 1a), which acts favorably for the coordination of Pb^{2+}.

Accordingly, due to the lack of the C═N groups in the L^2 ligand (Scheme 1b), the L^2/SPCE sensor displays very low sensitivity. The limit of detection (LoD), defined as LoD = 3.3 × SD/m,[40,41] where SD and m are the standard deviation of the blank and the slope of the calibration graph, respectively, obtained with the L^1/SPCE sensor is equal to 0.446 μM.

It is well known that the presence of noble metals can help in increasing the performances of the electrode material. For this, we further modified L^1/SPCE through the electrochemical deposition of Au nanoparticles as described in the Experimental section. The successful electrodeposition of AuNPs on L^1/SPCE was confirmed by the appearance of the characteristic oxidation and reduction peaks of gold observed at 0.9 V and 0.4 V, respectively (see Fig. 9).

The AuNP-L^1/SPCE sensor was then tested for the determination of Pb^{2+} (see Fig. 10a). The addition of AuNPs on the surface of the L^1/SPCE working electrode introduces an improvement in the electrooxidation performance toward Pb^{2+} ions, resulting in an almost double response with respect to that of the pristine L^1/SPCE sensor.

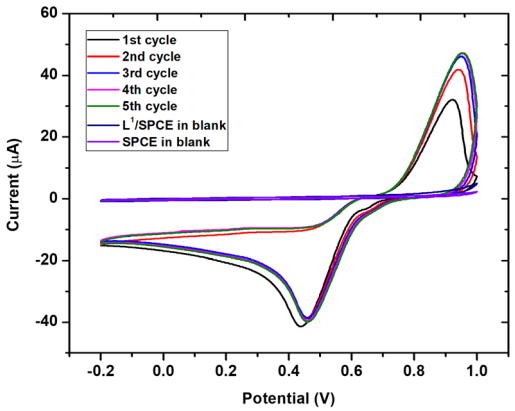

Fig. 9 Electrodeposition of AuNPs on L^1/SPCE using the cyclic voltammetry (CV) technique.

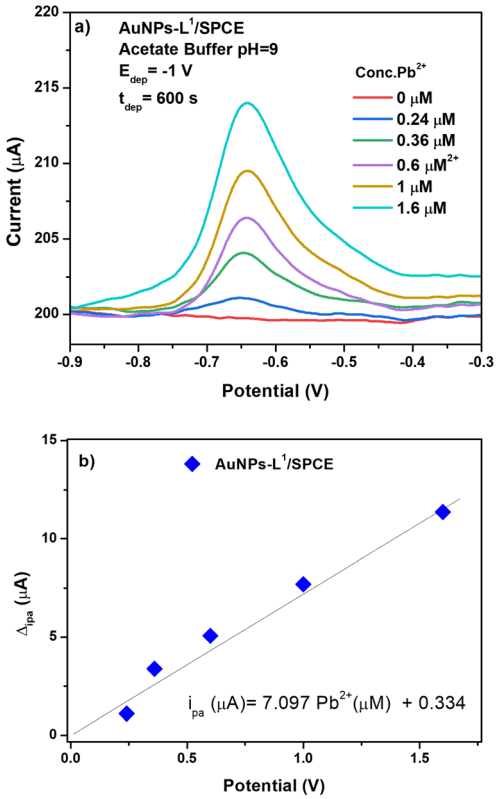

Fig. 10 SWASV voltammograms on (a) AuNPs-L^1/SPCE in an acetate buffer solution containing a low concentration of Pb(II) ions; conditions: pH = 9.0, E_{dep} = −1.0 V, and t_{dep} = 600 s. (b) Calibration curve.

From the calibration curve of AuNPs-L^1/SPCE (see Fig. 10b), the sensitivity has been calculated as i_{pa} (μA) = 7.097$C_{Pb^{2+}}$ (μM) + 0.334. The computed sensitivity of the sensor being 56.776 μA μM^{-1} cm^{-2} is higher than those reported for the other SPCEs (Fig. 8b). The calculated LoD value, at S/N ratio = 3, was 0.298 μM.

A scan rate variation study was performed to determine the controlling mechanism on the surface of AuNPs-L^1/SPCE. Tests were carried out in 5 mM $Fe(CN)_6$ in 0.1 mol L^{-1} KCl solution in the potential range [−0.2 V; 0.6 V] at different scan rates ranging from 0.02 V s^{-1} to 0.3 V s^{-1} (Fig. 11a). The increase of the scan rate leads to an increase in the anodic and cathodic current peaks labelled as i_{pa} and i_{pc}, respectively. As depicted in Fig. 11b, this increase is linear to the scan rate square root, with the regression equation i_{pa} (μA) = 164.805$V^{1/2}$ + 4.146 and R^2 = 0.98, proving that the electrooxidation on AuNP-L^1/SPCE is diffusion controlled. Based on this data, the electrochemically active surface area (EASA) is equal to 4.87 e^{-2} cm^2 and is determined using the following Randles–Sevcik formula:

$$I_{pa}\ (\text{in A}) = 2.69 \times 10^5 A D^{1/2} n^{3/2} v^{1/2} C.$$

where n is the number of electrons, C is the concentration in mol cm^{-3}, v is the scan rate, and D is the diffusion coefficient of the electrolyte equal to 7.6 × 10^{-6} cm^2 s^{-1}.

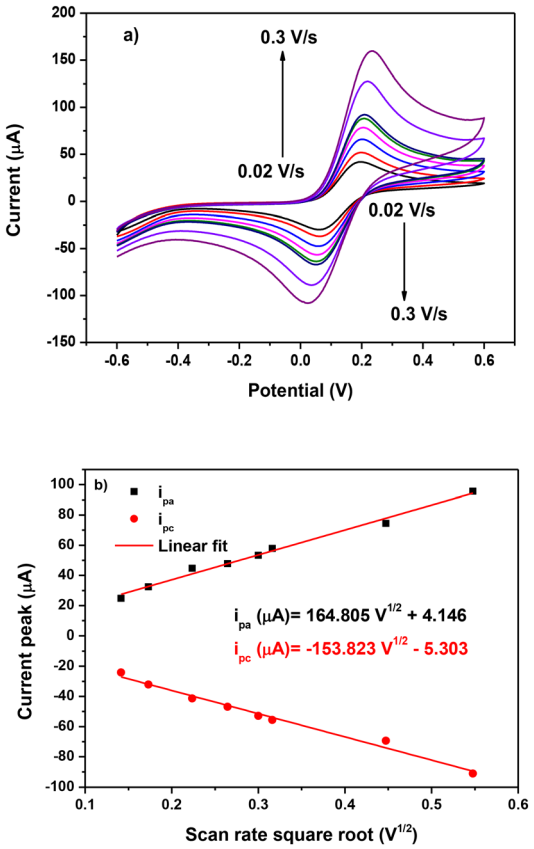

Fig. 11 (a) Scan rate variation study on AuNPs-L^1/SPCE and (b) linearity of the i_p current peak *vs.* scan rate square root.

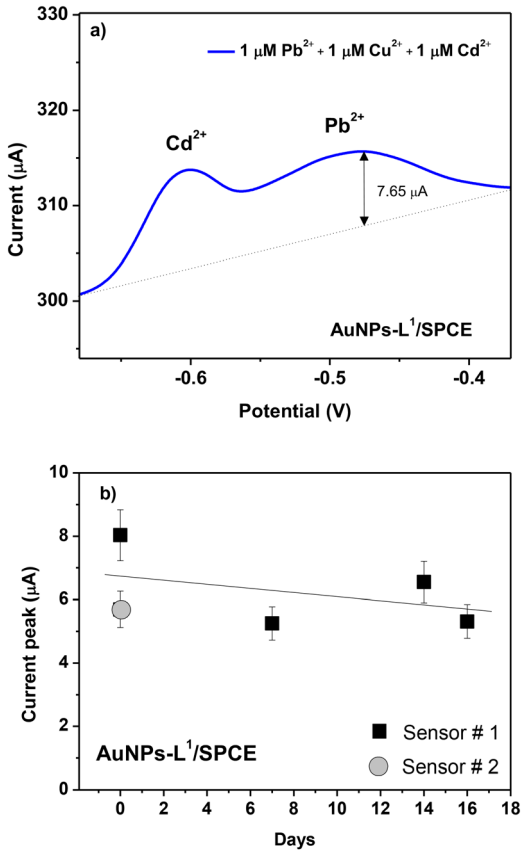

Fig. 12 (a) Selectivity test of the various HMI ions (Pb^{2+}, Cu^{2+}, and Cd^{2+}) at 1 μM in seawater and (b) reproducibility test of two AuNPs-L^1/SPCE sensors and signal stability test up to 16 days.

To study the selectivity of the proposed modified electrode, various HMIs such as Pb^{2+}, Cu^{2+}, and Cd^{2+} were tested under the same conditions (acetate buffer and pH = 9). Fig. 12a demonstrates that no oxidation peak is obtained in the blank sample. When adding 1 μM of Pb^{2+}, the expected oxidation peak is observed at −0.5 V. After adding 1 μM of Cu^{2+} and Cd^{2+}, a peak at −0.6 V is observed related to cadmium ions, whereas the peak intensity of Pb^{2+} is almost unchanged with respect to the expected current variation in the presence of Pb ions only, indicating that the tested interferents do not influence Pb ion determination.

Another important parameter for the sensor is also the stability feature. To study it, at 3-day time intervals up to 16 days, the SWAV technique is carried out on AuNPs-L^1/SPCE toward Pb^{2+} ions using the same conditions (Fig. 12b). Only a slight decrease of the current variation after about 2 weeks of operation can be observed, likely due to the poisoning of some sensitive sites by lead ions.

Real sample test on AuNPs-L^1/SPCE

As described in the Introduction section, the major goal of this investigation is the determination of Pb^{2+} in seawater. Thus, it is crucial to check the efficiency of the L^1-based SPCE sensor in a real seawater sample, collected from Messina, Italy. The sample, having a pH = 8.05, was used for the analysis as sampled and without any pre-treatment. The SWASV result is reported in Fig. 13. As expected, an increase in the current peak is observed when increasing the Pb^{2+} concentration. Based on the calibration curve previously determined, recovery rates determined by the spike-and-recovery experiment with 0.24, 0.36, and 0.6 μM of Pb^{2+} are found in the range of 98.3–111.3%, demonstrating the promising performances of the modified sensor for the

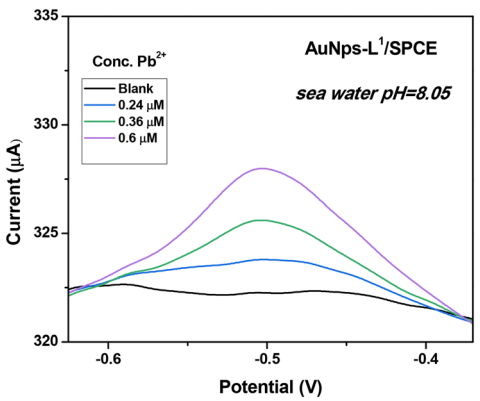

Fig. 13 Square-wave anodic stripping voltammograms (SWASVs) in seawater. Conditions: t_{dep} = 600 s and V_{dep} = −1 V.

detection of Pb^{2+} ions in real seawater with no sample treatment. Indeed, our electrochemical analysis pointed out that the concentration of Pb^{2+} naturally present in the seawater sample is negligible, as certified by independent analysis performed by means of atomic absorption spectroscopy.

Experimental

Reagents

The starting materials used were procured from Merck and Aldrich companies and used without any further purification unless otherwise stated. Lead nitrate was used to prepare the aqueous stock solution of the target heavy metals. Acetate buffer was prepared by combining acetic acid (0.1 M) and NaOH to achieve the desired pH. Double-distilled water was employed in all experimental procedures.

Apparatus

The ATR-FTIR spectra of the Schiff base ligands were recorded at a range of 4000–400 cm^{-1} employing a JASCO-680 model spectrometer. A spectrometer (JASCO-V570 model) was used for scanning the UV-visible spectra in a range of 200–800 nm. SEM analyses were carried out by means of a Zeiss (Gemini II model) microscope working at an acceleration voltage of 10 kV and at a working distance of 27 mm. ^1H NMR and ^{13}C NMR spectra were recorded using a Bruker DPX FT/NMR-400 spectrometer in the presence of tetramethylsilane (Me_4Si) as a standard and deuterated dimethyl sulfoxide (DMSO-d_6) as a solvent. The decomposition temperature or melting point and molar conductivity were measured using KRUSS SPIN melting point meters and a Metrohm-712 conductometer, respectively. A Perkin-Elmer Pyris model was used for the investigation of the thermal behavior of the compounds under a N_2 gas atmosphere within the temperature limit of 25–900 °C with a heating rate of 20 °C min^{-1}.

Electrochemical measurements were conducted through a commercially available screen-printed carbon electrode (SPCE) obtained from Metrohm-DropSens. The SPCEs consisted of a flat substrate with a carbon working electrode (4 mm in diameter, geometric area of 0.1257 cm^2), a silver pseudo reference electrode, and a carbon auxiliary electrode. Square wave anodic stripping voltammetry was performed using a DropSens μStat 400 Potentiostat, which was controlled using Dropview 8400 software for data acquisition.

Synthesis of Schiff base ligands L^1 and L^2

The L^1 and L^2 Schiff base ligands were prepared by following the same procedure used in our previous investigations.[36] Briefly, an ethanolic solution of 1,4-diaminobutane (0.044 g, 0.5 mmol) is dropwise added to 2-methoxycinnamaldehyde (0.161 g, 1 mmol) at 25 °C for 5 h (Scheme 1a). The purity is checked by thin-layer chromatography (TLC) and the reduction of the solvent volume allowed us to obtain yellow crystals of ligand L^1. The precipitate was collected, filtered, and washed with a small amount of ethanol and dried at room temperature.

The synthesis of the L^2 Schiff base ligand was carried out through the dropwise addition of an ethanolic solution of triethylenetetramine (0.073 g, 0.5 mmol) to an ethanolic solution of 4-dimethylaminocinnamaldehyde (0.175 g, 1 mmol) at 25 °C, (Scheme 1b). The reaction was carried out by stirring for five hours, and the purity of the synthesized Schiff base ligand (L^2) was confirmed using thin-layer chromatography (TLC). Upon reducing the solvent volume, a yellow precipitate of ligand L^2 formed. The precipitate was collected, filtered, and washed with a small amount of ethanol for further purification. Finally, ligand L^2 was dried at room temperature.[42] The prepared ligand was characterized using Fourier-transform infrared spectroscopy (FTIR) and nuclear magnetic resonance (NMR) spectroscopic techniques.

Preparation of modified electrodes

The bare screen-printed carbon electrodes (SPCEs) were used as received without any treatment performed before the use. To perform the modification of the working electrode, 1.0 mg of each of the ligand sample (L^1 and L^2) was ultrasonically dispersed in 0.5 mL of dimethyl sulfoxide (DMSO), and 2 μL of this suspension was dropped directly onto the surface of the carbon working electrode and dried at room temperature until further use.

AuNPs-L^1/SPCE is prepared through electrodeposition of AuNPs on the surface of the WE of L^1/SPCE. Herein, the modified electrode is immersed in 5 mL of $HAuCl^{4-}$ solution, and 5 cycles of cyclic voltammetry (CV) are carried out in the potential range [−0.2 V; 1 V] at a 0.05 V s^{-1} scan rate. The success of the electrodeposition is proved by the presence of Au oxidation and reduction peaks at 0.9 V and 0.4 V.

Electroanalytical analysis

Electrochemical studies were performed in 5 mL of acetate buffer solution to conduct square wave anodic stripping voltammetry (SWASV) measurements. Essential instrumental parameters, including pH and deposition potential/time (E_{dep}/t_{dep}), were optimized and determined to be pH = 9, −1 V, and 600 s, respectively. Following the preconcentration step, square wave voltammetry (SWV) was carried out in the voltage range of −1.5 V to 0 V to obtain the analytical signal corresponding to the concentration of the heavy metal ions.

Conclusions

In this work, a new sensor based on a bidentate (1*E*,1′*E*,2*E*,2′*E*)-*N*,*N*′-(butane-1,4-diyl)bis(3-(2-methoxyphenyl)prop-2-en-1-imine) Schiff-base ligand was developed for electrochemistry-based detection of Pb^{2+} in seawater. By combining AuNPs with this Schiff base ligand, a synergy was created leading to improved electrochemical sensing performances. Finally, the feasibility of the proposed platform for practical applications in the

environmental field was confirmed by determining Pb(II) in a seawater sample.

Data availability

The datasets generated and/or analysed in the current study are available from the authors upon reasonable request.

Author contributions

Z. Akbari: formal analysis and writing – editing. K. Abid, E. Fazio, C. Corsaro, and F. Neri: formal analysis and writing – review & editing. D. Iannazzo: project administration. M. Montazerozo: project administration. G. Neri: conceptualization and methodology.

Conflicts of interest

There are no conflicts to declare.

Acknowledgements

This work was supported by the European Union (NextGeneration EU) through the MUR-PNRR project SAMOTHRACE (No. ECS00000022).

References

1 B. Liu, J. Chai, S. Feng and B. Yang, Structure, photochemistry and magnetic properties of tetrahydrogenated Schiff base chromium(III) complexes, *Spectrochim. Acta, Part A*, 2015, **140**, 437–443.
2 Z. Akbari, M. Montazerozohori, S. Joohari, P. Hayati, N. Micale and M. Cristani, *et al.*, Mono and binuclear cadmium complexes: X-ray crystal structures, Hirshfeld surface analysis and antimicrobial/antioxidant studies, *Inorg. Chem. Commun.*, 2023, **158**, 111513.
3 F. N. Ejiah, M. O. Rofiu, O. A. Oloba-Whenu and T. M. Fasina, Schiff bases as analytical tools: synthesis, chemosensor, and computational studies of 2-aminophenol Schiff bases, *Mater. Adv.*, 2023, **4**(10), 2308–2321.
4 Z. Akbari, M. Montazerozohori, S. J. Hoseini and R. Naghiha, Ultrasonic assisted preparation of some new zinc complexes of a new tetradentate Schiff base ligand: thermal analyses data, antimicrobial and DNA cleavage potential, *J. Phys. Org. Chem.*, 2021, **34**(5), e4180.
5 Z. Akbari, M. Montazerozohori, S. J. Hoseini, R. Naghiha, P. Hayati and G. Bruno, *et al.*, Synthesis, crystal structure, Hirshfeld surface analyses, antimicrobial activity, and thermal behavior of some novel nanostructure hexa-coordinated Cd(II) complexes: Precursors for CdO nanostructure, *Appl. Organomet. Chem.*, 2021, **35**(5), e6181.
6 Z. Akbari, C. Stagno, N. Iraci, T. Efferth, E. A. Omer and A. Piperno, *et al.*, Biological evaluation, DFT, MEP, HOMO-LUMO analysis and ensemble docking studies of Zn(II) complexes of bidentate and tetradentate Schiff base ligands as antileukemia agents, *J. Mol. Struct.*, 2024, **1301**, 137400.
7 Y. W. Choi, J. J. Lee, E. Nam, M. H. Lim and C. Kim, A fluorescent chemosensor for Al3+ based on julolidine and tryptophan moieties, *Tetrahedron*, 2016, **72**(16), 1998–2005.
8 Z. Liu, H. Xu, L. Sheng, S. Chen, D. Huang and J. Liu, A highly selective colorimetric and fluorescent chemosensor for Al(III) based-on simple naphthol in aqueous solution, *Spectrochim. Acta, Part A*, 2016, **157**, 6–10.
9 H. M. Park, B. N. Oh, J. H. Kim, W. Qiong, I. H. Hwang and K. D. Jung, *et al.*, Fluorescent chemosensor based-on naphthol–quinoline for selective detection of aluminum ions, *Tetrahedron Lett.*, 2011, **52**(43), 5581–5584.
10 A. Barba-Bon, A. M. Costero, S. Gil, M. Parra, J. Soto and R. Martínez-Máñez, *et al.*, A new selective fluorogenic probe for trivalent cations, *Chem. Commun.*, 2012, **48**(24), 3000.
11 A. Salmanipour and M. A. Taher, An electrochemical sensor for stripping analysis of Pb(II) based on multiwalled carbon nanotube functionalized with 5-Br-PADAP, *J. Solid State Electrochem.*, 2011, **15**(11–12), 2695–2702.
12 D. A. Atwood, Cationic group 13 complexes, *Coord. Chem. Rev.*, 1998, **176**(1), 407–430.
13 Z. Akbari, M. Montazerozohori, G. Bruno, K. Moulaee and G. Neri, Development of a novel electrochemical nitrite sensor based on Zn-Schiff base complexes, *Appl. Organomet. Chem.*, 2022, **36**(4), e6610.
14 A. Afkhami, H. Bagheri, H. Khoshsafar, M. Saber-Tehrani, M. Tabatabaee and A. Shirzadmehr, Simultaneous trace-levels determination of Hg(II) and Pb(II) ions in various samples using a modified carbon paste electrode based on multi-walled carbon nanotubes and a new synthesized Schiff base, *Anal. Chim. Acta*, 2012, **746**, 98–106.
15 A. Afkhami, H. Ghaedi, T. Madrakian and M. Rezaeivala, Highly sensitive simultaneous electrochemical determination of trace amounts of Pb(II) and Cd(II) using a carbon paste electrode modified with multi-walled carbon nanotubes and a newly synthesized Schiff base, *Electrochim. Acta*, 2013, **89**, 377–386.
16 A. Afkhami, F. Soltani-Felehgari, T. Madrakian, H. Ghaedi and M. Rezaeivala, Fabrication and application of a new modified electrochemical sensor using nano-silica and a newly synthesized Schiff base for simultaneous determination of Cd2+, Cu2+ and Hg2+ ions in water and some foodstuff samples, *Anal. Chim. Acta*, 2013, **771**, 21–30.
17 A. García-Miranda Ferrari, P. Carrington, S. J. Rowley-Neale and C. E. Banks, Recent advances in portable heavy metal electrochemical sensing platforms, *Environ. Sci.: Water Res. Technol.*, 2020, **6**(10), 2676–2690.
18 A. Aravind, M. Sebastian and B. Mathew, Green synthesized unmodified silver nanoparticles as a multi-sensor for Cr(III) ions, *Environ. Sci.: Water Res. Technol.*, 2018, **4**(10), 1531–1542.
19 A. G. M. Ferrari, P. Carrington, S. J. Rowley-Neale and C. E. Banks, Recent advances in portable heavy metal electrochemical sensing platforms, *Environ. Sci.: Water Res. Technol.*, 2020, **6**(10), 2676–2690.
20 M. S. Collin, S. K. Venkatraman, N. Vijayakumar, V. Kanimozhi, S. M. Arbaaz and R. G. S. Stacey, *et al.*, Bioaccumulation of lead (Pb) and its effects on human: A review, *J. Hazard. Mater. Adv.*, 2022, **7**, 100094.

21 S. Pourbeyram, S. Fathalipour, B. Rashidzadeh, H. Firuzmand and B. Rahimi, Simultaneous determination of Cd and Pb in the environment using a pencil graphite electrode modified with polyaniline/graphene oxide nanocomposite, *Environ. Sci.: Water Res. Technol.*, 2023, **9**(12), 3355–3365.

22 X. Liu, Y. Yao, Y. Ying and J. Ping, Recent advances in nanomaterial-enabled screen-printed electrochemical sensors for heavy metal detection, *TrAC, Trends Anal. Chem.*, 2019, **115**, 187–202.

23 D. Wu, Y. Hu, H. Cheng and X. Ye, Detection Techniques for Lead Ions in Water: A Review, *Molecules*, 2023, **28**(8), 3601.

24 V. Bressi, Z. Akbari, M. Montazerozohori, A. Ferlazzo, D. Iannazzo and C. Espro, *et al.*, On the Electroanalytical Detection of Zn Ions by a Novel Schiff Base Ligand-SPCE Sensor, *Sensors*, 2022, **22**(3), 900.

25 P. B. Tchounwou, C. G. Yedjou, A. K. Patlolla and D. J. Sutton, Heavy metal toxicity and the environment, *Exper. Suppl.*, 2012, **101**, 133–164.

26 B. Bansod, T. Kumar, R. Thakur, S. Rana and I. Singh, A review on various electrochemical techniques for heavy metal ions detection with different sensing platforms, *Biosens. Bioelectron.*, 2017, **94**, 443–455.

27 M. Kumar Goshisht, G. Kumar Patra and N. Tripathi, Fluorescent Schiff base sensors as a versatile tool for metal ion detection: strategies, mechanistic insights, and applications, *Mater. Adv.*, 2022, **3**(6), 2612–2669.

28 J. Acharya, U. Kumar and P. M. Rafi, Removal of Heavy Metal Ions from Wastewater by Chemically Modified Agricultural Waste Material as Potential Adsorbent-A Review, *Int. J. Curr. Eng. Technol.*, 2018, **28**, 526–530.

29 S. Afroze and T. K. Sen, A Review on Heavy Metal Ions and Dye Adsorption from Water by Agricultural Solid Waste Adsorbents, *Water, Air, Soil Pollut.*, 2018, **229**(7), 225.

30 Q. Ding, C. Li, H. Wang, C. Xu and H. Kuang, Electrochemical detection of heavy metal ions in water, *Chem. Commun.*, 2021, **57**(59), 7215–7231.

31 C. Z. Zhang, B. Chen, Y. Bai and J. Xie, A new functionalized reduced graphene oxide adsorbent for removing heavy metal ions in water via coordination and ion exchange, *Sep. Sci. Technol.*, 2018, **53**(18), 2896–2905.

32 A. S. Ahmed, M. B. I. Mohamed, M. A. Bedair, A. A. El-Zomrawy and M. F. Bakr, A new Schiff base-fabricated pencil lead electrode for the efficient detection of copper, lead, and cadmium ions in aqueous media, *RSC Adv.*, 2023, **13**(23), 15651–15666.

33 R. Kumar Saren, S. Banerjee, B. Mondal, S. Senapati and T. Tripathy, An electrochemical sensor–adsorbent for lead (Pb 2+) ions in an aqueous environment based on Katiragum–Arginine Schiff base, *New J. Chem.*, 2022, **46**(41), 19740–19750.

34 C. Mohan, K. Sharma and S. Chandra, Lead (II)-Selective Potentiometric Sensor Based on Thiophene-2-Aldehyde Thiosemicarbazone (TATS) Schiff Base in PVC Matrix, *Anal. Bioanal. Electrochem.*, 2022, **14**(9), 860–870.

35 M. Rashid, R. Kouser, F. Arjmand and S. Tabassum, New graphene oxide-loaded probe as a highly selective fluorescent chemosensor for the detection of iron ions in water samples using optical methods, *Opt. Mater.*, 2023, **142**, 114077.

36 Z. Akbari, M. Montazerozohori, R. Naghiha, P. Hayati, N. Micale and M. Cristani, *et al.*, Some new antimicrobial/antioxidant nanostructure zinc complexes: Synthesis, crystal structure, Hirshfeld surface analyses and thermal behavior, *Results Chem.*, 2022, **4**, 100636.

37 G. Wu, M. Li, J. Zhu, K. W. Chiu Lai, Q. Tong and F. Lu, A highly sensitive and selective turn-on fluorescent probe for Pb(ii) ions based on a coumarin–quinoline platform, *RSC Adv.*, 2016, **6**(103), 100696–100699.

38 B. A. Mei, O. Munteshari, J. Lau, B. Dunn and L. Pilon, Physical Interpretations of Nyquist Plots for EDLC Electrodes and Devices, *J. Phys. Chem. C*, 2018, **122**, 194–206.

39 H. S. Magar, R. Y. A. Hassan and A. Mulchandani, Electrochemical Impedance Spectroscopy (EIS): Principles, Construction, and Biosensing Applications, *Sensors*, 2021, **21**(19), 6578.

40 M. Khan, K. Abid, A. Ferlazzo, V. Bressi, C. Espro and M. Hussain, *et al.*, A Sensitive and Selective Non-Enzymatic Dopamine Sensor Based on Nanostructured Co3O4–Fe2O3 Heterojunctions, *Chemosensors*, 2023, **11**(7), 379.

41 K. Abid, A. Foti, A. Khaskhoussi, C. Celesti, C. D'Andrea and P. Polykretis, *et al.*, A study of Screen-Printed Electrodes Modified with MoSe2 and AuNPs-MoSe2 Nanosheets for Dopamine Sensing, *Electrochim. Acta*, 2023, 143371.

42 Z. Akbari, M. Montazerozohori, S. J. Hoseini, R. Naghiha, P. Hayati and G. Bruno, *et al.*, Synthesis, crystal structure, Hirshfeld surface analyses, antimicrobial activity, and thermal behavior of some novel nanostructure hexa-coordinated Cd(II) complexes: Precursors for CdO nanostructure, *Appl. Organomet. Chem.*, 2021, **35**(5), e6181.

